Analysis of the Fluid–Structure Interaction in the Optimization-Based Design of Polymer Sheeting Dies

Qi Wang, Douglas E. Smith

Department of Mechanical and Aerospace Engineering, University of Missouri, Columbia, Missouri 65211

Received 11 July 2006; accepted 26 September 2006
DOI 10.1002/app.25517
Published online in Wiley InterScience (www.interscience.wiley.com).

ABSTRACT: A polymer-sheeting-die-design methodology is presented that integrates a simulation of the polymer melt flow and die-cavity deformation with numerical optimization to compute a die-cavity geometry capable of giving a nearly uniform exit flow rate. Both the polymer melt flow and sheeting-die deformation are analyzed with a general-purpose finite-element program. The approach includes a user-defined element that is used to evaluate the purely viscous non-Newtonian flow in a flat die. The flow analysis, which is simplified with the Hele–Shaw approximation, is coupled to a three-dimensional finite-element simulation for die deformation. In addition, shape optimization of a polymer sheeting die is performed by the incorporation of the coupled analyses in our constrained optimization algorithm. A sample problem is discussed to illustrate the die-design methodology. © 2006 Wiley Periodicals, Inc. J Appl Polym Sci 103: 3994–4004, 2007

Key words: extrusion; polyethylene (PE); simulations

INTRODUCTION

The analysis and design of the polymer extrusion process used to produce thin sheets and films have received much attention over the last few decades, but only a few reports have appeared in the literature that analyze the die deformation.[1,2] It is well known that high internal pressure within the viscous polymer flow causes die deformation, which can have a significant effect on the flow distribution in the die and the melt velocity over the die exit. As a result, die designs that neglect die-body deformation may not perform as desired.

The primary focus of most sheet- or slit-die designs is the development of a uniform velocity across the width of the die exit. Various design approaches have been applied to T-dies, fish-tail dies, and coat-hanger dies in which the cross-section geometry of the distribution manifold is defined over the width of the die to yield a uniform exit velocity.[3] Sheeting dies have also been designed on the basis of one-dimensional (1D) flow for slowly reacting polymeric liquids.[4] Recently, sheeting-die designs have been computed with two-dimensional (often called 2.5D) melt flow simulations with an isothermal power-law fluid, a Carreau–Yasuda fluid, and other more complicated generalized Newtonian fluid models.[5,6] Sartor[7] was perhaps the first to combine numerical optimization with a two-dimensional (2D) flow network analysis to iteratively solve the die-design problem with a power-law fluid model. Smith et al.[8] developed a finite-element simulation based on the Hele–Shaw flow approximation similar to that used in injection-molding simulations.[9] More recently, Smith and Wang[6] extended the earlier optimization approaches to include various generalized Newtonian fluid models, and they addressed variability in die design by including an adjustable choker bar in the melt flow analysis and design.[10] In both of their articles, constraints were defined to measure the die's exit-velocity variation, and design sensitivity expressions were developed that greatly reduced the computational effort required in the design-optimization calculations.

The flow of a polymer melt in sheeting dies has also been evaluated with three-dimensional (3D) flow equations with numerical approaches, such as the finite-element method, to solve for the pressures, velocities, and temperatures in the flow.[11–14] These simulations have assumed isothermal flow, which is justified in part by the work of Pittman and Sander.[15] Also considered are coextrusion,[12] wall slip,[13] and die swell.[14] More recently, numerical optimization methods have been combined with 3D melt flow simulations, which provide a powerful technique for designing die cavities.[16,17] This type of design methodology allows a more general definition of the die cavity and may include more complex flow fields and constitutive behavior. Unfortunately, these efforts have mostly focused on die-cavity-design problems without considering the influence of die-body deformation.

Correspondence to: D. E. Smith (SmithDoug@Missouri.edu).
Contract grant sponsor: National Science Foundation; contract grant number: DMI-0327732.

It is well understood that die-body deformation has a strong effect on the design and operation of extrusion dies, but surprisingly, it has received relatively little attention in the literature. Previous work includes a 1D flow analysis and a deformation analysis, but they ignored the effect that the melt pressure has on the deformation of the die body.[18,19] More recently, Sander and Pittman[1] developed a fully coupled approach, using a 2.5D Hele–Shaw flow simulation to calculate the melt pressure and a 2D thick-plate analysis for die deflection. The predicted results agreed closely with experimental data for a die with a relatively simple internal flow channel and die-body geometry. However, Sander and Pittman avoided the full 3D analysis and more complex die geometry ''because of their high computational demands''.[1] A 3D flow analysis coupled with a full 3D die-deformation analysis appears in Gifford's work.[2] Unfortunately, this earlier approach required specialized software to evaluate the polymer flow within the die and to include the effect of die deformations. Furthermore, the computational efforts required to obtain more accurate 3D solutions can be excessive when used in an iterative design procedures, particularly when applied to detailed industrial designs.

This article considers an optimization-based approach for designing polymer extrusion dies in which the die-cavity geometry is computed to minimize the die-inlet pressure (P_{in}) while delivering a uniform exit flow rate. The proposed approach enhances previous design methodologies by incorporating the flow analysis and 3D die-deformation analysis in the optimization-based design methodology. Die deformation is analyzed in this approach with the general-purpose finite-element program ABAQUS[20] which is also used to solve the generalized Hele–Shaw flow equation for an isothermal Carreau–Yasuda fluid to obtain the pressure field on the internal surface of the die body. Upon the completion of the coupled fluid–structure interaction analysis, Sequential Quadratic Programming (SQP) in Design Optimization Tools (DOT)[21] is used to solve the optimization problems. An example of a coat-hanger die is provided to demonstrate the proposed methodology.

MELT FLOW GOVERNING EQUATION

The Hele–Shaw flow model can be derived from the principles of conservation of mass, momentum, and energy to provide a simplified governing equation for non-Newtonian and inelastic flows in thin cavities.[9] In this analysis, inertial, body, and surface-tension forces in the fluid are assumed to be negligible. Moreover, the pressure does not vary significantly in the direction normal to the plane of flow, the die-cavity thickness is assumed to be small in comparison with its in-plane dimensions and has little in-plane variation, and all flow conditions are assumed to be symmetric with respect to the cavity midplane. The Hele–Shaw model is widely employed in injection and compression molding[22] and has also been applied to sheet extrusion dies.[6,7,8,23–26]

On the basis of these assumptions, the mass and momentum conservation equations reduce to a single differential equation:[22]

$$\nabla \cdot S \nabla P = 0 \tag{1}$$

where P is the pressure field over the die cavity in two dimensions and ∇ is the gradient operator in the plane of flow. S is the flow conductance defined in terms of the viscosity, η, as an integral through the cavity thickness:[22]

$$S = \int_0^h \frac{z^2}{\eta(\dot{\gamma}(z))} dz \tag{2}$$

where h is the half-height of the die cavity and coordinate z is normal to the plane of flow. η is a function of the strain-rate magnitude, $\dot{\gamma}$, which is computed for the generalized Hele–Shaw analysis at distance z from the midplane:

$$\dot{\gamma} = \frac{z}{\eta} \|\nabla P\| \tag{3}$$

where ($\|\nabla P\|$) is the magnitude of the pressure gradient. The boundary conditions in the plane of flow are $P = P_{in}$ and $P = 0$ at the die inlet and exit, respectively. We impose $\partial P/\partial n = 0$ on impermeable boundaries and symmetry planes, where $\partial/\partial n$ denotes the normal derivatives.

This study employs the Carreau–Yasuda fluid model to define the non-Newtonian dependence of η on $\dot{\gamma}$. The Carreau–Yasuda model exhibits near-Newtonian behavior at low strain rates and captures the power-law decay in η as the strain rate increases. It can be written as follows:[27]

$$\eta = \eta_\infty + (\eta_0 - \eta_\infty)\left[1 + (\lambda\dot{\gamma})^a\right]^{(n-1)/a} \tag{4}$$

where η_0 is the zero-shear-rate viscosity, η_∞ is the infinite-shear-rate viscosity, λ is a time constant, n is the power-law index, and a is an empirically derived material constant. $\eta_\infty = 0$ and $a = 2$ are typical for a polymer melt.[28] Equation (2) cannot be evaluated analytically when the Carreau–Yasuda fluid model is employed. The analysis is further complicated because η, defined in eq. (4), is a function of $\dot{\gamma}$ through eq. (3) in the generalized Hele–Shaw formulation. To solve the example to follow, we evaluate S in eq. (2) numerically with an eight-point Gaussian quadrature, for which η, defined through eqs. (3) and (4), is computed at a given value of z with a local Newton–Raphson iteration, as described elsewhere.[6]

The residual, R, for the boundary value problem described in eq. (1) is obtained via the method of weighted residuals[29] in the usual manner (e.g., ref. 23):

$$R(P) = \int_{\Omega} \nabla\omega \cdot S(P)\nabla P \, d\Omega \tag{5}$$

where ω is an arbitrary weighting function and we have assumed that there is no prescribed flow rate on the boundary of the 2D flow domain, Ω. When non-Newtonian fluids are evaluated, S in eq. (2) becomes a function of P, and eq. (5) is nonlinear in P, requiring iterative methods to compute a solution. In this research, the nonlinear system of equations derived from R appearing in eq. (5) is solved via the Newton–Raphson iteration method because it exhibits terminal quadratic convergence. The tangent operator, $\partial R/\partial P$, acting on the increment, $[\Delta P]$, is obtained by the differentiation of eq. (5) with respect to P:

$$\frac{\partial R}{\partial P}[\Delta P] = \int_{\Omega} \nabla\omega \left[S\nabla[\Delta P] + \frac{\partial S}{\partial P}[\Delta P]\nabla P \right] d\Omega \tag{6}$$

Equation (2) is differentiated to obtain

$$\frac{\partial S}{\partial P}[\Delta P] = -\int_0^h \frac{z^2}{\eta^2} \frac{\partial \eta}{\partial P}[\Delta P] dz \tag{7}$$

Furthermore, eqs. (3) and (4) are differentiated with respect to P, and following some mathematical manipulations, we obtain $\partial\eta/\partial P$ appearing in eq. (7):

$$\frac{\partial \eta}{\partial P}[\Delta P] = \left[\frac{(n-1)(\lambda\dot{\gamma})^a \eta(\eta - \eta_\infty)}{\eta + (\lambda\dot{\gamma})^a(\eta_\infty + n(\eta - \eta_\infty))} \right] \frac{\nabla P \cdot \nabla[\Delta P]}{\|\nabla P\|^2} \tag{8}$$

The isoparametric finite-element method (e.g., ref. 29) can be used to discretize the residual and tangent operator in eqs. (5) and (6), respectively, and related terms from eqs. (7) and (8). In the finite-element analysis, P and R become the nodal pressure vector, $\mathbf{P}$, and the residual vector, $\mathbf{R}$, respectively. In a similar manner, $\partial R/\partial P$ in eq. (6) becomes the tangent matrix, $\partial\mathbf{R}/\partial\mathbf{P}$. Once the residual and tangent matrix are evaluated with the finite-element method, the nodal-pressure-vector increment, $\Delta\mathbf{P}$, is computed at iteration $\mathbf{I}$ with the Newton–Raphson method:

$$\frac{\partial \mathbf{R}(\mathbf{P_I})}{\partial \mathbf{P}} \Delta\mathbf{P} = -\mathbf{R}(\mathbf{P_I}) \tag{9}$$

The nodal pressures are updated as $\mathbf{P_{I+1}} = \mathbf{P_I} + \Delta\mathbf{P}$. Iterations are repeated until convergence is reached. Once the pressure solution is obtained, the gapwise average velocity, $\bar{\mathbf{v}}$, is computed from

$$\bar{\mathbf{v}} = -\frac{S}{h}\nabla P \tag{10}$$

In this work, eqs. (5)–(6) are discretized with the Galerkin finite-element method and then solved with the general-purpose finite-element program ABAQUS with a user-defined element (UEL).[20] In this approach, P within the die cavity is computed at each node with Newton–Raphson iterations.

COUPLED ANALYSIS WITH FLUID/STRUCTURE INTERACTION

It is clear that for a proper simulation of the die design, it is necessary to couple the analysis of the flow distribution and pressure field in the die cavity with the analysis of the die-body deformation. Indeed, the high internal pressure within the melt flow causes die deformation, which, in turn, alters the pressure field. Figure 1 illustrates the iterative computational methodology used to solve the coupled fluid–structure analysis. The coupled analysis loop starts with the initialization of pressures and nodal heights. These values are included in an input file of the finite-element program together with a UEL subroutine to calculate the nodal pressure solution. To better serve the 3D simulation in the finite-element program, the nodal pressures are translated into surface pressures. The resulting surface pressures are then interpolated onto the mesh surface of the die's internal channel, and the linear elastic deformation of the die is calculated, corresponding to those pressure loads.

The deformation caused by the melt pressure forces the die channel to open; thus, the new and deformed heights of the flow channel are generated. The newly generated heights are then interpolated back to the Hele–Shaw model to recalculate the pressure solution. As the die flow channel opens, the change in pressure in the die between iterations will decrease, reducing the tendency of further deformation.[2] The iterative loop presented here normally takes three or four iterations to converge in our example, as shown in Figure 2. To reduce the computational time, an automatic algorithm is developed in this work to compute the coupled pressure solutions and die deformation, and the overall simulation based on this automatic algorithm can run on a personal computer with only a few minutes of calculation.

COAT-HANGER DIE FLOW AND DEFORMATION EXAMPLE

The sheeting-die design considered in this article is derived from the coat-hanger die, which is commonly used in industrial applications and widely studied and tested experimentally.[6,23,30] The specific

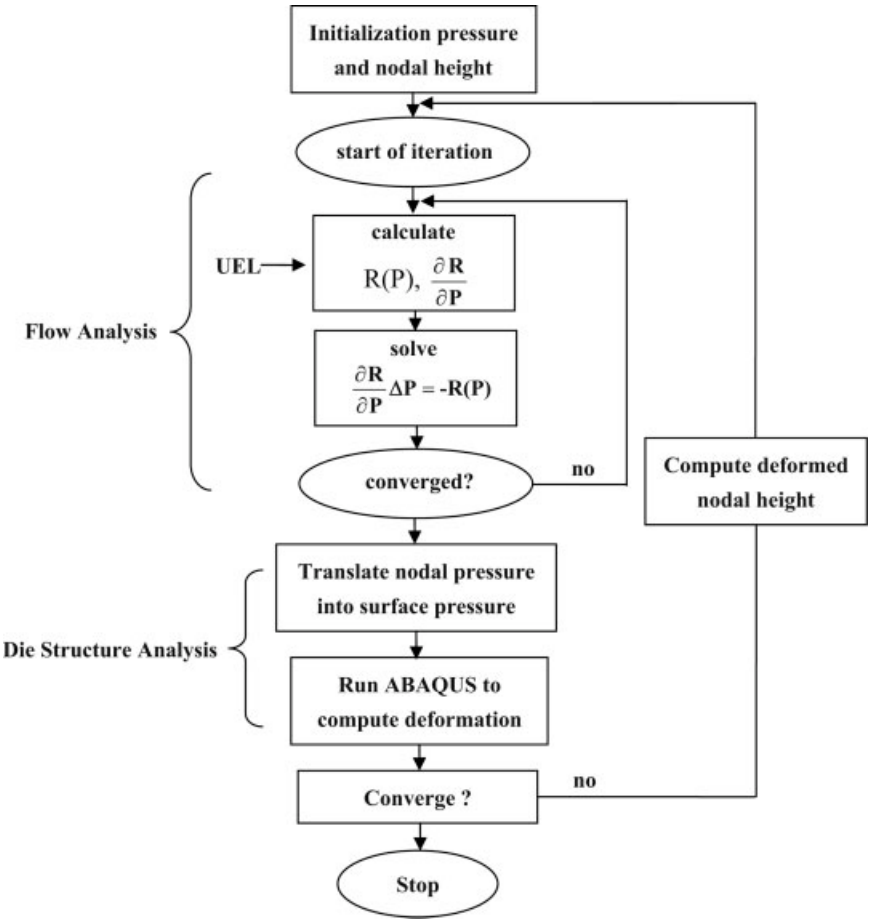

Figure 1 Computational procedure for the coupled fluid–structure analysis.

die geometry used in this study is shown in Figure 3; it is symmetric about the die's centerline (i.e., $x = 0$) and is similar to that presented elsewhere by Gifford.[13] It consists of four major regions, as shown in Figure 3: the manifold, preland, secondary manifold, and land. The purpose of the manifold is to distribute the polymer melt uniformly across the die. The secondary manifold and the land each have a uniform cavity half-height and act as resistance to the flow, which provides better flow uniformity.[28]

The land defines the thickness of the polymer melt immediately exiting the die. The dimensions that define our die-cavity geometry are taken from Table I of Gifford,[13] except for the land gap, which is fixed at 1.6 mm (i.e., die-exit half-height $h_{exit} = 0.8$ mm) for the initial design in this article. The total die-exit width is 1016 mm, which results in an exit-width-to-height aspect ratio of 635. The die-inlet gap and width are 19.05 and 101.6 mm, respectively, and the total die length (including the inlet channel) is 330 mm, which includes the 137-mm-long inlet channel. The land, secondary manifold, and preland lengths along the die centerline are 25.4, 50.8, and 50.8 mm, respectively. There is a flow channel along the top of the die in the manifold region, which has a uniform half-height in the y direction and a centerline length of 15.2 mm. The manifold also includes a region having a centerline length of 50.8 mm with a half-height that decreases linearly in the y direction between the flow channel and the die preland. For illustration, the finite-element mesh in Figure 4 represents the entire flow domain, in which the flow channel is modeled

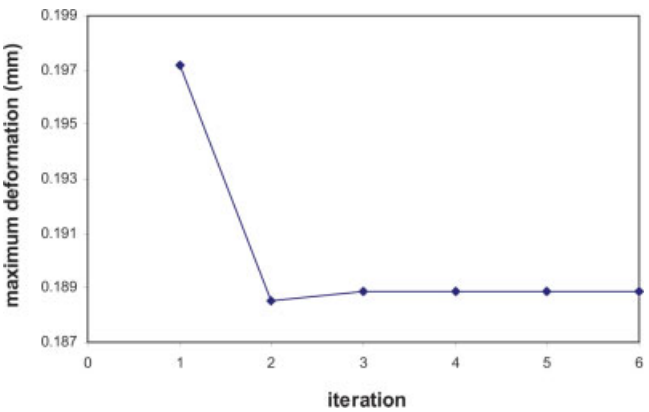

Figure 2 Typical iteration history of the maximum deformation of the die body. [Color figure can be viewed in the online issue, which is available at www.interscience.wiley.com.]

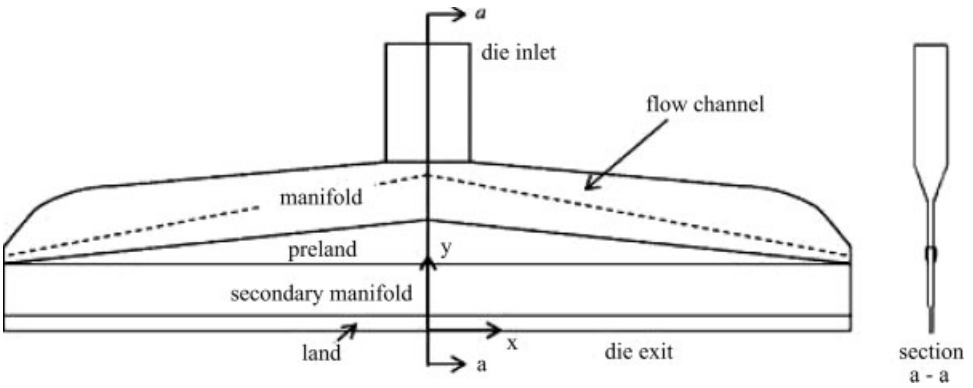

Figure 3 Coat-hanger die-cavity geometry.

with three-node triangular elements; however, all the calculations to follow are performed with a half-symmetry model in $x \geq 0$ (not shown) having 853 nodes and 1558 elements.

The flow of low-density polyethylene at 270°C is selected at which material constants $\eta_0 = 800$ Pa-s, $\eta_\infty = 0$, $\lambda = 0.02129$ s, $n = 0.45958$, and $a = 2$ are taken from Gifford.[2] P_{in} is defined as 10 MPa, whereas the outlet is defined as the zero pressure along die exit. The cavity thickness is defined at each node. The die-body geometry is determined by the parameters listed in Table I of Gifford.[2] The die is assumed to be constructed of carbon steel with a Young's modulus of 2.068×10^{11} Pa and a Poisson's ratio of 0.3. Figure 5 shows the finite-element mesh of one-half of the die body with 109,060 elements containing 24,072 nodes. The coat-hanger die used here has two planes of symmetry. Therefore, we only consider one quadrant of the die in the structural analysis.

Figure 6 shows the deformed die-body geometry after the convergence is reached. Because of the plane of symmetry, only a quarter of the die-body geometry is shown in Figure 6. The highest deformation occurs at the center position of the die exit, at which h is increased by 23.6% from 0.8 to 0.989 mm. The pressure distributions in the die for the undeformed and deformed die bodies are shown in Figure 7(a,b), respectively. As expected, when the die deformation is included in the simulation, the pressure distribution across the die will change such that the pressure decreases in the die as the die flow channel opens up. Additionally, pressure isobars along the die-exit region for the undeformed die body are more uniform than those for the deformed die body. This is because the largest deformation occurs at the center position of the die exit, causing the lower pressure at the center and higher pressure at the edge of the die exit.

TABLE I
Initial and Optimal Design Variables and Performance Measures

	Die design	
	Initial	Optimal
Design variables		
$\phi_1 = P_{in}$ (MPa)	10.0	6.57
ϕ_2 (mm)	3.2	12.64
ϕ_3 (mm)	12.05	18.23
ϕ_4 (mm)	5.2	17.32
ϕ_5 (mm)	3.0	3.08
ϕ_6 (mm)	3.5	3.75
ϕ_7 (mm)	4.0	12.23
Constraint		
g_1	1.34	0.00013
Exit flow rates per unit of width (mm^2/s)		
Average	736.0	347.3
Maximum	853.6	364.2
Minimum	452.2	290.5

SHEETING-DIE-DESIGN OPTIMIZATION

In the die-design-optimization problem considered in this study, the pressure drop across the die and the die-exit-flow-rate variation define the success of a given die design. These criteria are chosen because the pressure drop determines the extruder size and power requirements and the die-exit-flow-rate variation influences the sheet thickness uniformity. The goal of minimizing P_{in} can be realized by the variation of the thickness distribution in the die cavity while a constraint is placed on the die-exit-flow-rate variation and the slope of the die cavity surface in the manifold region is limited. The nonlinear constrained die-design-optimization problem can be stated in terms of the design variable vector, ϕ, as follows:

$$\begin{aligned} &\text{Determine : } \phi \\ &\text{To minimize : } f(\phi) = P_{in} \\ &\text{Subject to : } g_1(\phi) = \frac{1}{L}\int_{l_{exit}} \left(\frac{q(x,\phi)}{q_p} - 1\right)^2 dx \leq \varepsilon \\ &\qquad g_2(\phi) = \text{MAX}\left(\frac{dh(x)}{dx}\right) \leq 0 \\ &\qquad \phi_i^L \leq \phi_i \leq \phi_i^U \end{aligned} \tag{11}$$

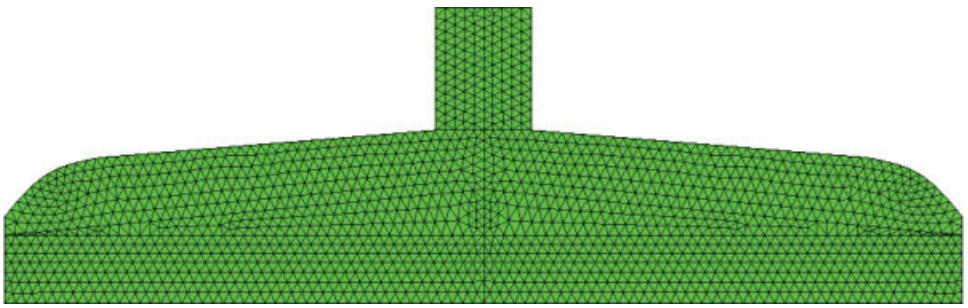

Figure 4 Finite-element mesh of the polymer melt flow domain. [Color figure can be viewed in the online issue, which is available at www.interscience.wiley.com.]

where l_{exit} denotes the die-exit edge. P_{in} is minimized. This cost function represents the pressure drop through the die because we fix the outlet pressure (P_{out}) at 0. Constraint function g_1 measures the exit-flow-rate variation and is imposed to obtain a uniform exit flow rate within the tolerance, ε. In g_1, $q(x,\phi)$ is the exit flow rate per unit of width, and q_p is the desired exit flow rate per unit of width. When $q(x,\phi)$ equals q_p across the entire die exit, the die is operating at the desired total flow rate, Q, which is determined as follows:

$$Q = 2\int_{l_{exit}} q(x,\phi)dx \tag{12}$$

In the manifold region of the die cavity, the half-height parameter, $h(x)$, is arbitrary, so constraint g_2 is imposed to restrict the slope of h in the x direction to be less than zero. In the aforementioned optimization problem, ϕ is the design variable vector with real components $\phi_i (i = 1, 2, \ldots N$, where N is the total number of design variables), limited by upper and lower bounds ϕ_i^U and ϕ_i^L, respectively. In addition, h in the flow channel is constrained to decrease along the centerline of the die.

COAT-HANGER DIE DESIGN EXAMPLE

In this example, the sheeting-die-design problem has $N = 7$ design variables that are included in ϕ. P_{in} is defined by the design as $P_{in} = \phi_1$ and is bounded by 1.0 MPa $\leq P_{in} \leq$ 20 MPa. In addition, the half-heights in the preland, manifold, and secondary manifold regions shown in Figure 3 are defined by the remaining six design variables. The half-height in the preland region is defined as a constant, ϕ_2. h in the manifold flow channel along the top of the die is defined by the Lagrange interpolating polynomial in x:

$$h(x) = \frac{(x - L/2)(x - L)}{L^2/2}h_0 + \frac{(x)(x - L)}{-L^2/4}\phi_3 + \frac{(x)(x - L/2)}{L^2/2}\phi_4 \tag{13}$$

where $L = 508$ mm is the die half-width and h_0 is the die half-height at $x = 0$. Design variables ϕ_3 and ϕ_4 in eq. (13) are the manifold half-heights at $x = L/2$ and $x = L$, respectively. The slope of h in the manifold region of the die cavity is evaluated from eq. (13) as follows:

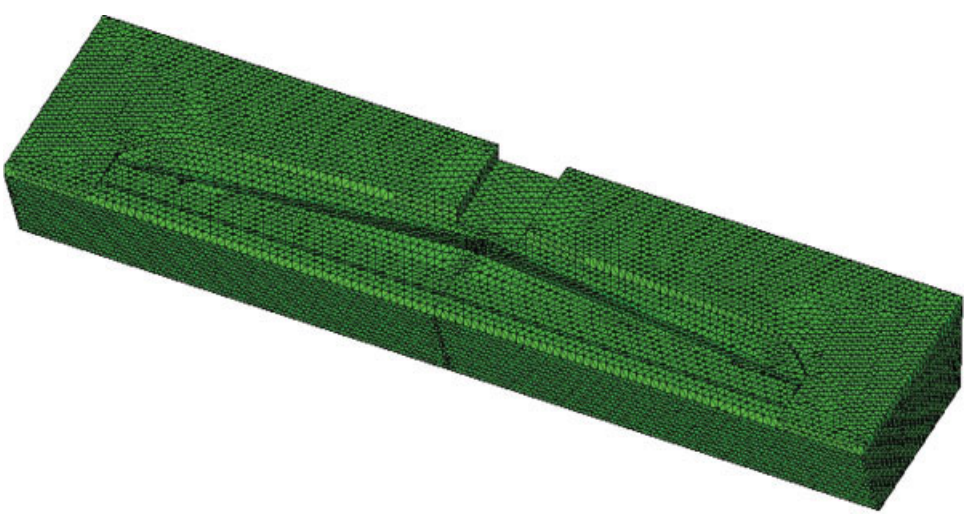

Figure 5 Half-symmetry of the finite-element mesh of the undeformed die body. [Color figure can be viewed in the online issue, which is available at www.interscience.wiley.com.]

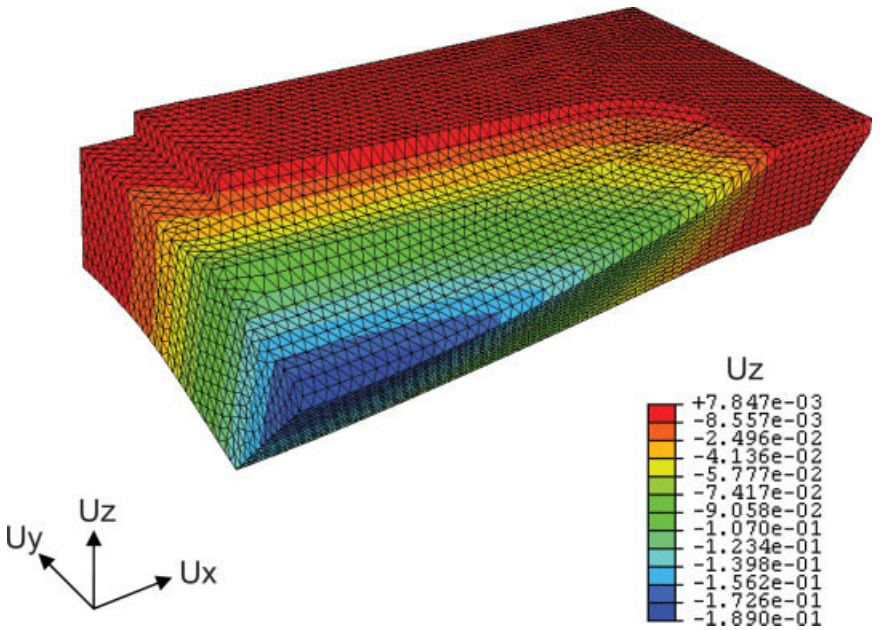

Figure 6 Displacement magnitude of the die body (deformation scale factor = 336). [Color figure can be viewed in the online issue, which is available at www.interscience.wiley.com.]

$$\frac{dh(x)}{dx} = \frac{2x - 1.5L}{L^2/2}h_0 + \frac{2x - L}{-L^2/4}\phi_3 + \frac{2x - L/2}{L^2/2}\phi_4 \quad (14)$$

This is constrained by g_2 in eq. (11). h in the secondary manifold region is defined by a cubic polynomial:

$$h(x) = \phi_5 + (-7.0\phi_5 + 8.0\phi_6 - \phi_7)\left(\frac{x}{L}\right)^2 + (6.0\phi_5 - 8.0\phi_6 + 2.0\phi_7)\left(\frac{x}{L}\right)^3 \quad (15)$$

where $dh/dx = 0$ is imposed at $x = 0$. In eq. (15), the

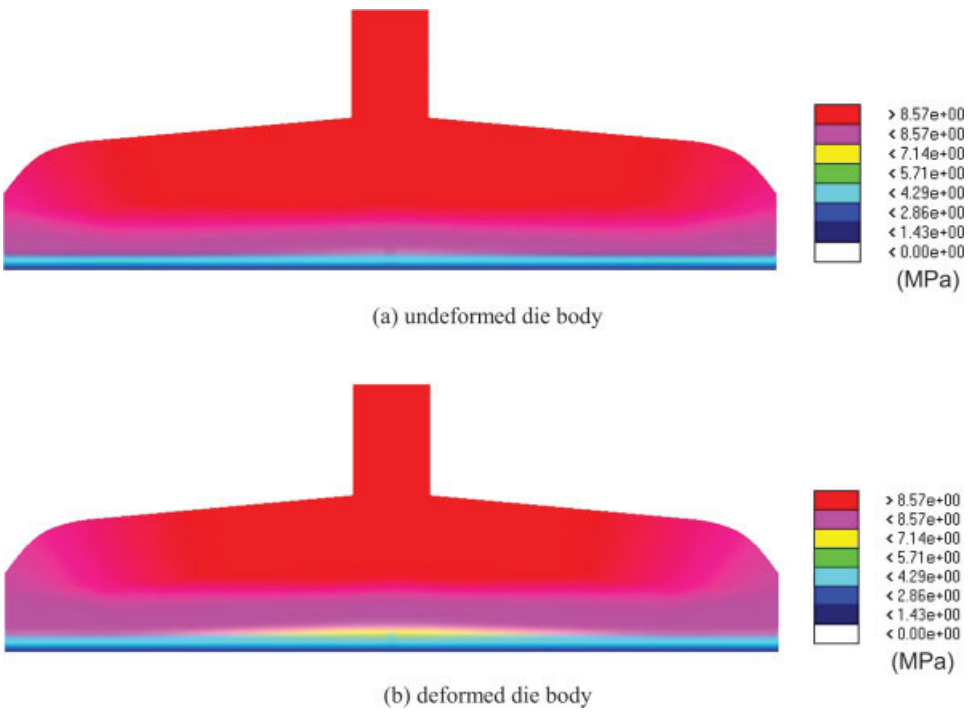

Figure 7 Pressure distribution in the die cavity. [Color figure can be viewed in the online issue, which is available at www.interscience.wiley.com.]

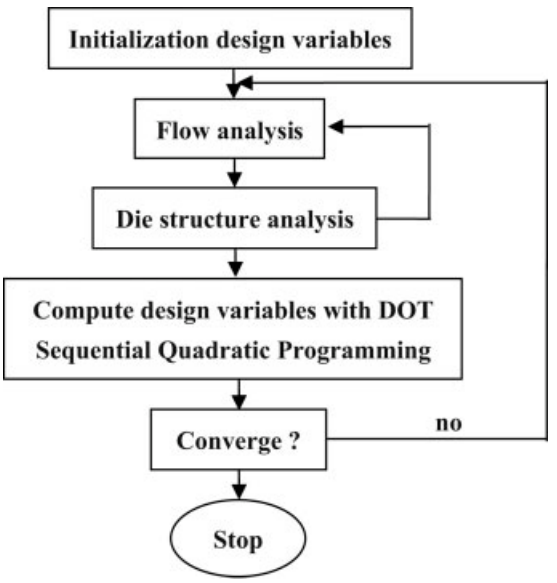

Figure 8 Computational procedure for die-design optimization.

design variables ϕ_5, ϕ_6, and ϕ_7 are the secondary manifold half-heights at $x = 0$, $x = L/2$, and $x = L$, respectively. The secondary manifold region can be treated as a choker bar for which $h(x,y)$ can be adjusted independently; this assumes that an operator, or perhaps an automatic control device, can make an adjustment for flow conditions considered to facilitate the optimal die flow operation. All half-height design variables are bounded by 1.0 mm $\leq \phi_k \leq$ 19.05 mm ($k = 2, 3, \ldots N$) in the die-optimization problem. The desired exit flow rate per unit of width is $q = 350$ mm^2/s for the flow condition considered in eq. (11). Also, the exit-flow-rate tolerance for g_1 in eq. (11) is defined as $\varepsilon = 0.0015$.

The computational procedure of die-design optimization is shown in Figure 8, which includes the coupled fluid–structure interaction in the die-design problem. Starting with initial values of the design variables, the computer program calculates the pressure and die-cavity half-height in a coupled analysis. The values of the deformed die-cavity half-heights are compared with the previous values until convergence is reached. Upon completion of the coupled fluid–structure analysis loop, a new design variable, ϕ, is computed with the DOT SQP algorithm.[21]

RESULTS AND DISCUSSION

A new design has been computed with the DOT SQP algorithm[21] in 19 optimization iterations with gradients computed via the forward finite-difference approximation. The optimization results for the die design are summarized in Table I. The optimal history for P_{in} appears in Figure 9(a), and the value of constraint g_1 in eq. (11) is shown in Figure 9(b) at each optimization iteration. In these calculations, the pressure drop decreases from 10 to 6.57 MPa, a 34.3% reduction, whereas the exit-flow-rate constraint, g_1, is reduced considerably from its initial value of 1.34 to its optimal value of 0.00013, which is well below ε. Changes in the design variables are also shown in Table I. The uniformity in the exit flow rate is evidenced by the reduction in the difference between the maximum and minimum gapwise-exit-velocity values. Moreover, the optimal average exit flow rate per unit width is near the desired value of 350 mm^2/s.

The pressure distributions in the midplane of the initial and optimal designs are shown in Figure 10(a,b), respectively. When the die deformation is included in the design simulation, the die pressure decreases as the die channel opens up. Since the

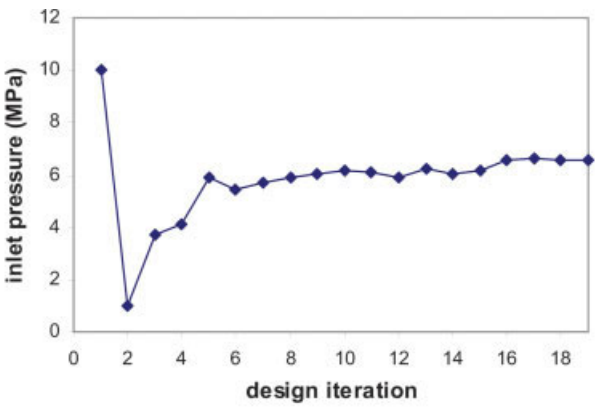

(a) objective function optimization history

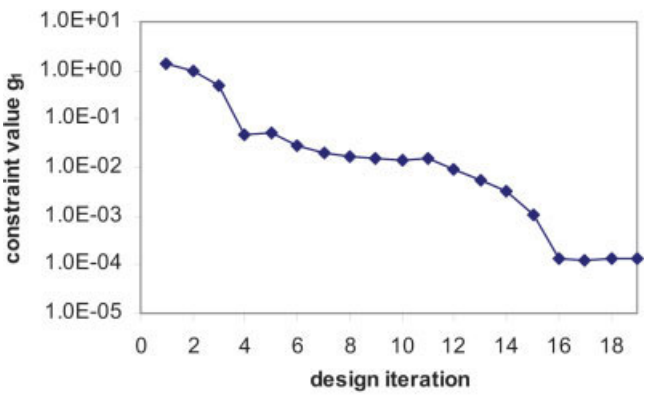

(b) optimization history for exit flow rate constraint

Figure 9 Design iteration history for the objective function and exit-flow-rate constraint. [Color figure can be viewed in the online issue, which is available at www.interscience.wiley.com.]

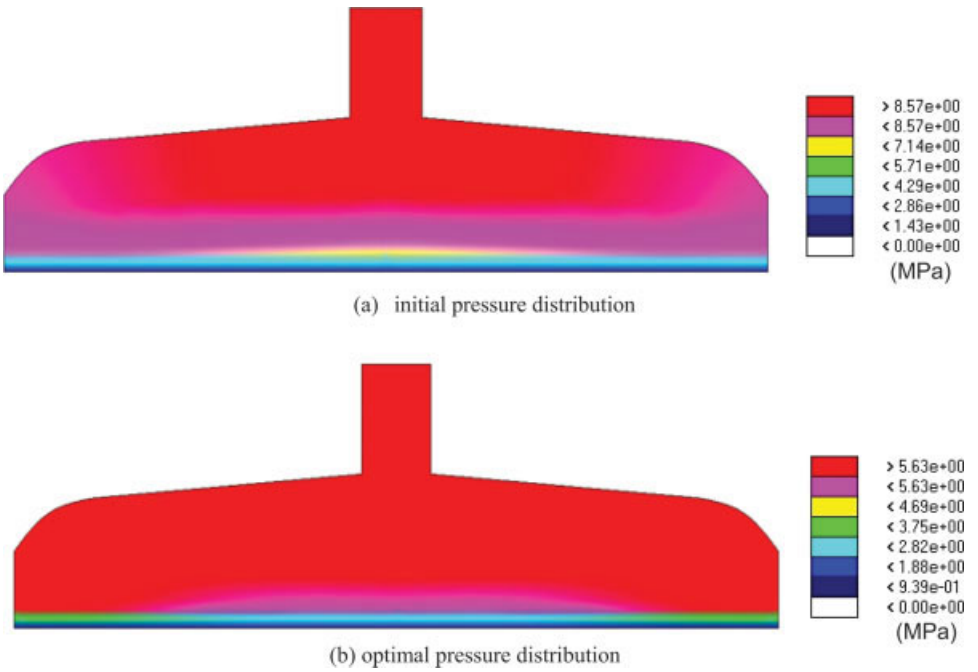

Figure 10 Pressure distribution in the die cavity. [Color figure can be viewed in the online issue, which is available at www.interscience.wiley.com.]

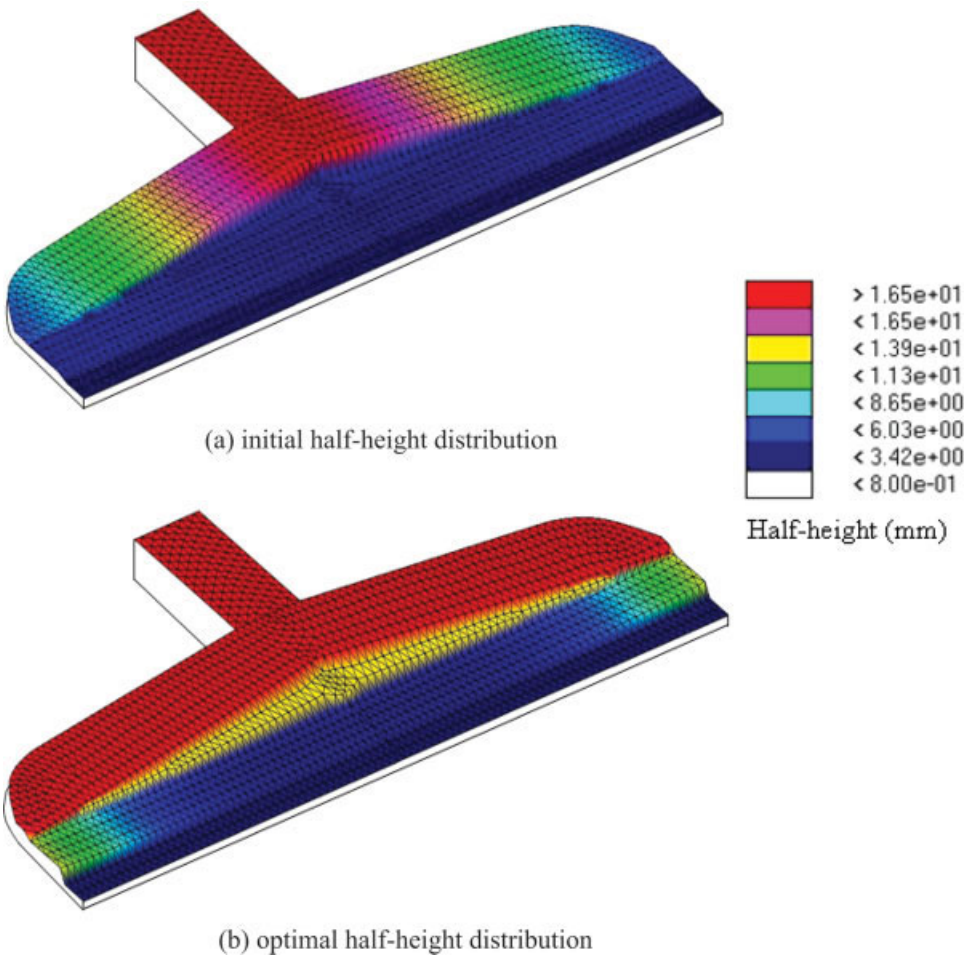

Figure 11 Die-cavity half-height distributions. [Color figure can be viewed in the online issue, which is available at www.interscience.wiley.com.]

half-heights along the die exit are no longer uniform because of the gap opening, the pressure isobars will not be parallel to the die exit. As expected, the isobars just inside the die exit of the initial design are more parallel than those of the optimal design, as shown in Figure 10(a,b), respectively. The die-cavity half-heights are presented in Figure 11(a) for the initial design and in Figure 11(b) for the optimal design. The gap-thickness in the manifold and prel- and regions of the optimal design are increased in comparison with that of the initial design. The half-height changes can also be seen in the secondary manifold region (i.e., choker bar).

Die-exit flow rates are illustrated for the initial and optimal designs in Figure 12, in which the distance along the die exit is normalized with the exit width. The exit flow rates for the initial design are far from the desired value and show a significantly higher flow rate along the centerline of the die than at its edge. The optimal die design provides a more uniform exit flow rate, which illustrates how well the design approach is able to meet the desired flow rate over the entire width of the die. Figure 13 shows the die-exit flow rate and velocity distribution for the optimal design and is provided here to illustrate the influence of die deformation on the uniformity of the flow distribution. The exit flow rate is the product of the die-exit half-height and velocity. For the uniform exit flow rate, the exit velocity will decrease as the half-height increases. The die-exit half-height, which is initially uniform across the die exit, increases more in the center, resulting in a lower velocity than that at the die's outer edge. Compared with the exit-velocity distribution, the flow rate is more uniform. As can be seen in the plot, the optimal design generates a nearly uniform flow rate distribution at the die exit.

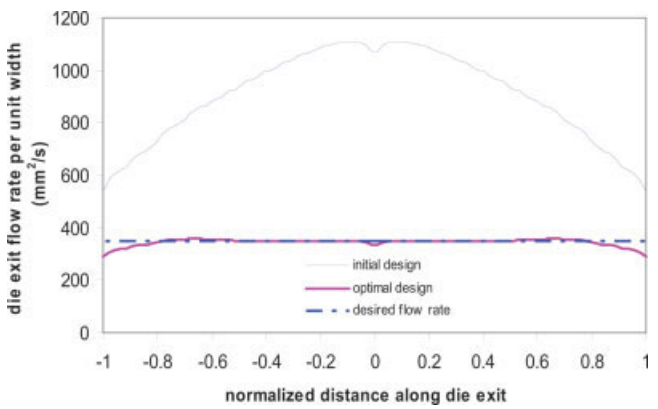

Figure 12 Exit flow rate for the coat-hanger die design. [Color figure can be viewed in the online issue, which is available at www.interscience.wiley.com.]

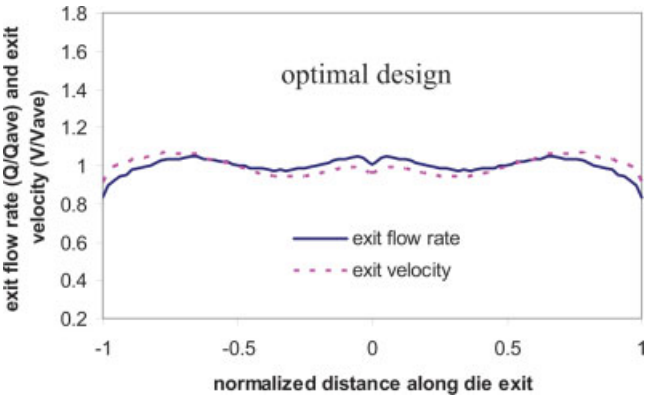

Figure 13 Effect of the die deformation on the exit flow distribution. [Color figure can be viewed in the online issue, which is available at www.interscience.wiley.com.]

CONCLUSIONS

An optimization-based polymer-sheeting-die-design methodology has been presented in this article, and performance measures in the optimization have been evaluated with a coupled flow analysis and 3D simulation of die deformation. In this approach, sheeting dies are analyzed with a general-purpose finite-element program, in which a user element program is developed to evaluate the purely viscous non-Newtonian flow in a die. An automatic algorithm to calculate the coupled pressure and die deformation has been presented, and a sheeting-die-design-optimization problem has illustrated the design approach.

References

1. Sander, R.; Pittman, J. F. T. Polym Eng Sci 1996, 36, 1972.
2. Gifford, W. A. Polym Eng Sci 1998, 38, 1729.
3. Winter, H. H.; Fritz, H. G. Polym Eng Sci 1986, 26, 543.
4. Pan, J. P.; Wu, P. Y.; Liu, T. J. Polym Eng Sci 1997, 37, 856.
5. Liu, T.-J.; Liu, L.-D. Polym Eng Sci 1994, 34, 541.
6. Smith, D. E.; Wang, Q. Polym Eng Sci 2005, 45, 953.
7. Sartor, L. Ph.D. Thesis, University of Minnesota, 1990.
8. Smith, D. E.; Tortorelli, D. A.; Tucker, C. L. Comput Methods Appl Mech Eng 1998, 167, 283.
9. Kennedy, P. Flow Analysis of Injection Molds; Hanser: New York, 1995.
10. Smith, D. E.; Wang, Q. J Manufacturing Sci Eng 2006, 128, 11.
11. Dooley, J. Soc Plast Eng Annu Tech Conf Tech Pap 1990, 36, 168.
12. Gifford, W. A. Polym Eng Sci 2000, 40, 2095.
13. Gifford, W. A. Polym Eng Sci 2001, 41, 1886.
14. Gifford, W. A. Polym Eng Sci 2003, 43, 1657.
15. Pittman, J. F. T.; Sander, R. Int Polym Process 1994, 9, 326.
16. Nobrega, J.; Carneiro, O. S.; Pinho, F. T.; Oliveria, P. J. Soc Plast Eng Annu Tech Conf Tech Pap 2002, 48, 122.
17. Nobrega, J.; Pinho, F.; Oliveria, P.; Carneiro, O. Soc Plast Eng Annu Tech Conf Tech Pap 2003, 49, 310.
18. Helmy, H. J Plast Film Sheeting 1987, 4, 193.
19. Michaeli, W. Extrusion Dies for Plastics and Rubber, 2nd ed.; Hanser: New York, 1992.

20. ABAQUS/Standard User's Manual; Hibbitt, Karlsson, and Sorensen: Pawtucket, RI, 2002.
21. DOT User's Manuals; Vanderplaats Research and Development: Colorado Springs, CO, 2001.
22. Hieber, C. A.; Shen, S. F. J Non-Newtonian Fluid Mech 1980, 7, 1.
23. Smith, D. E. Int J Numer Methods Eng 2003, 57, 1381.
24. Wen, S. H.; Liu, T. J. Polym Eng Sci 1995, 35, 759.
25. Smith, D. E. Soc Plast Eng Annu Tech Conf Tech Pap 2003, 49, 315.
26. Bates, S. J.; Pittman, J. F. T.; Sienz, J.; Langley, D. S. Polym Eng Sci 2003, 43, 1500.
27. Tadmor, Z.; Gogos, C. G. Principles of Polymer Processing; Wiley: New York, 1979.
28. Baird, D. G.; Collias, D. I. Polymer Processing: Principles and Design; Butterworth-Heinemann: Newton, MA, 1995.
29. Huebner, K. H.; Dewhirst, D. L.; Smith, D. E.; Byrom, T. G. The Finite Element Method for Engineers, 4th ed.; Wiley: New York, 2001.
30. Smith, D. E.; Wang, Q. AIAA Pap 2004, 45, 1959.